

# Fabrication and characterization of suspended beam structures for SiO<sub>2</sub> photonic MEMS

Tjitte-Jelte Peters and Marcel Tichem

Precision and Microsystems Engineering, Delft University of Technology, Mekelweg 2, 2628 CD Delft, Netherlands

E-mail: [t.j.peters@tudelft.nl](mailto:t.j.peters@tudelft.nl)

Received 22 January 2015, revised 16 July 2015

Accepted for publication 23 July 2015

Published 26 August 2015



## Abstract

This paper proposes a microfabrication process for the reliable release of SiO<sub>2</sub> beam structures. These structures are intended to be utilized in SiO<sub>2</sub> photonic MEMS. A major fabrication challenge is the release of thick (>10 μm) SiO<sub>2</sub> structures with high yield. A single mask process is developed based on temporary reinforcement of the SiO<sub>2</sub> structure. A supporting layer of Si functions as a reinforcing layer during etching and release, thereby enabling a high fabrication yield. Furthermore, the process allows to create structures of which the final Si support thickness is configurable from tens of micrometers to zero, thereby providing additional design freedom.


The fabrication process is tested on a silicon wafer with a ~15 μm thick thermal oxide layer. The obtained suspended structures are mechanically characterized. Two deformation effects can be distinguished: a curvature of the beam and a slope at the base of the beam. These effects are caused by the compressive mean stress and the gradient stress in the thermal SiO<sub>2</sub>. The curvature of the SiO<sub>2</sub>-Si beams corresponds to a concave downward profile while the SiO<sub>2</sub> beams without supporting Si reveal a small curvature in the opposite direction (concave upward). The slope at the base is approximately -0.5° for the SiO<sub>2</sub> beams and between -0.5° and 0° for the SiO<sub>2</sub>-Si beams. The acquired bending stiffness of long SiO<sub>2</sub> beams is in the newton per meter range (e.g. 0.8 N m<sup>-1</sup> for a cantilever measuring 1000 μm in length and 13 μm in width).

Keywords: stress, beam curvature, waveguide, bending stiffness, silicon dioxide MEMS

(Some figures may appear in colour only in the online journal)

## 1. Introduction

Silicon (Si) has been extensively studied and used as a construction material for micro electro mechanical systems (MEMS), because of its favorable mechanical and electrical properties. Si is a mechanically strong and elastic material, contributing to reliable micromechanical devices. Moreover, Si is stable up to high temperatures and has a tunable electrical conductivity.

 Content from this work may be used under the terms of the [Creative Commons Attribution 3.0 licence](https://creativecommons.org/licenses/by/3.0/). Any further distribution of this work must maintain attribution to the author(s) and the title of the work, journal citation and DOI.

However, Si is not necessarily the material of choice for microsystems with optical functionality. Other material systems deliver better photonic performance. An example is a stoichiometric silicon nitride (Si<sub>3</sub>N<sub>4</sub>) waveguide core encapsulated in a silicon dioxide (SiO<sub>2</sub>) cladding [1], showing a propagation loss which is lower than that of a Si waveguide. A similar Si<sub>3</sub>N<sub>4</sub>-SiO<sub>2</sub> waveguide configuration is applied in the TriPleX technology [2]. The means are available to realize functionally complex photonic integrated circuits (PICs) based on these and other material systems.

The waveguides in PICs are mostly buried in or created atop a solid layer. If suspended and mechanically flexible

waveguide beams can be created, this will open up entirely new possibilities, combining the advantages of MEMS with the preferred optical performance of photonic material systems. In earlier work, we have proposed an alignment concept for the alignment of the waveguides of two PICs, based on suspended TriPleX waveguides and integrated MEMS actuators [3]. This alignment concept and comparable SiO<sub>2</sub> photonic MEMS applications require the development of fabrication processes for realizing mechanical structures in SiO<sub>2</sub>. This paper addresses the challenges in creating such structures and proposes a method for their high-yield fabrication.

The fabrication of structures for SiO<sub>2</sub> photonic MEMS is challenging because of the thickness of the layer. The use of SiO<sub>2</sub> as a construction material which at the same time has good optical properties requires thick SiO<sub>2</sub> cladding layers. A total thickness of approximately 15 μm is required for a Si<sub>3</sub>N<sub>4</sub>-SiO<sub>2</sub> photonic waveguide with acceptable propagation loss. This thickness differs from the thickness required for other uses of SiO<sub>2</sub>. For example, when used as a dielectric material or as a (local) doping/etching mask, a thin (<1 μm) layer of SiO<sub>2</sub> suffices.

The principle of suspended photonic waveguides has already been demonstrated in literature. Suspended waveguides have been fabricated using various materials, e.g. polymer [4], InP [5], and Si [6]. While some research groups have described the release of SiO<sub>2</sub> structures, the obtained structures have different properties than we aim for. Carpenter *et al* [7] reported on the fabrication of suspended SiO<sub>2</sub> cantilevers, but the structures were produced by flame hydrolysis deposition instead of thermal oxidation. Ollier [8] described the fabrication of suspended SiO<sub>2</sub> structures made of PECVD SiO<sub>2</sub> instead of thermal SiO<sub>2</sub>. The SiO<sub>2</sub> cantilevers fabricated by Chen *et al* [9] are in the thickness range from 4 μm to 6 μm and therefore do not meet our thickness requirements. It is important to mention that both Ollier [8] and Chen *et al* [9] included additional lateral beams in their design in order to reduce stress-induced out-of-plane bending of the structure. Wang [10] successfully released 2 μm thick thermal SiO<sub>2</sub> with no additional lateral beams. The suspended SiO<sub>2</sub> structures were instead supported by a 28 μm–38 μm thick layer of Si.

Reports on suspended structures realized out of SiO<sub>2</sub> with a thickness around 15 μm were not found in literature. In our prior work [3], we demonstrated that the release of 15 μm thick SiO<sub>2</sub> waveguide beams is hindered by beam failure due to compressive stress. When SiO<sub>2</sub> is released from its Si substrate, the compressive stress is converted into strain. If a SiO<sub>2</sub> structure is confined (e.g. in a doubly clamped beam situation), the strain will lead to buckling and the resulting stress concentrations can cause beam failure.

This paper offers a robust method to create >10 μm thick suspended SiO<sub>2</sub> structures. These suspended structures are an essential element of our proposed alignment concept and the development of SiO<sub>2</sub>-based MEMS technology in general. The enabling technology and microfabrication process are explained in section 2. Section 3 presents and discusses the results of the proposed Si reinforcement method. Fabricated devices include suspended SiO<sub>2</sub> structures with and without

Si support. Furthermore, the feasibility of positioning the suspended SiO<sub>2</sub> structures with microactuators is evaluated by estimating the beam spring constants and the beam curvature. Section 4 presents the conclusions.

## 2. Technology

### 2.1. Fabrication process

The realization of suspended SiO<sub>2</sub>-Si (henceforth referred to as bilayer) beam structures is accomplished by plasma etching both the SiO<sub>2</sub> and the Si. Plasma etching is preferred over wet etching for releasing a suspended structure, to prevent stiction due to surface tension driven adhesion.

In this study, we describe the release of thermal SiO<sub>2</sub> structures. The results of releasing suspended TripleX structures are expected to be comparable to those obtained with thermal SiO<sub>2</sub> structures, since the dominant factor leading to beam fracturing is the mean residual stress. Thermal SiO<sub>2</sub> has a compressive mean residual stress resembling that of the TriPleX stack.

Figure 1 presents the steps of the single mask fabrication process. The starting material is a Si wafer with a thickness of ~525 μm and a 14.8 μm thick thermal SiO<sub>2</sub> layer. A 6 μm-thick spray-coated layer of AZ9260 photoresist was applied on top of the SiO<sub>2</sub> and patterned. The design of the photolithography mask allows control over in-plane dimensional parameters like the width and the length of the waveguide beams. The SiO<sub>2</sub> was etched using a Drytek Triode 384T with C<sub>2</sub>F<sub>6</sub>-CHF<sub>3</sub> chemistry (figure 1(b)). After etching through the SiO<sub>2</sub> layer, the photoresist mask was not removed but was used once more to etch trenches in the Si (figure 1(c)). From this fabrication step on, an SPTS Omega i2L Rapier deep silicon etcher was used, unless stated otherwise. A trench depth of ~70 μm was realized by deep reactive ion etching (DRIE) and the trench width varied from 30 μm to 100 μm.

After etching the trench in the Si, a ~1 μm thick passivation layer was deposited (figure 1(d)), which was then locally removed from the trench bottom by directional ion bombardment (figure 1(e)). The CF<sub>x</sub> passivation layer was deposited using C<sub>4</sub>F<sub>8</sub> gas. SF<sub>6</sub> gas and 75 W platen HF power were applied during the trench bottom removal. With the Si sidewalls protected, the Si underneath the beams was then removed by isotropic plasma etching (figure 1(f)). During this etch, SF<sub>6</sub> was used without applying any platen HF power. Removal of the passivation layer and photoresist mask by an O<sub>2</sub> plasma in a Tepla 300 plasma system resulted in suspended bilayer structures (figure 1(g)). As long as bilayer structures are required, no further processing is needed. In this study, the supporting Si was completely removed by performing additional fabrication steps. Another isotropic plasma etching step with SF<sub>6</sub> gas was performed for 60 s, reducing the Si reinforcement (figure 1(h)). All the supporting Si was then removed by a final isotropic plasma etch of 210 s using SF<sub>6</sub> (figure 1(i)). Two separate isotropic Si etch steps were performed to enable intermediary measurements.

The advantage of Si reinforcement can be demonstrated by comparing the release of a beam structure with and without Si

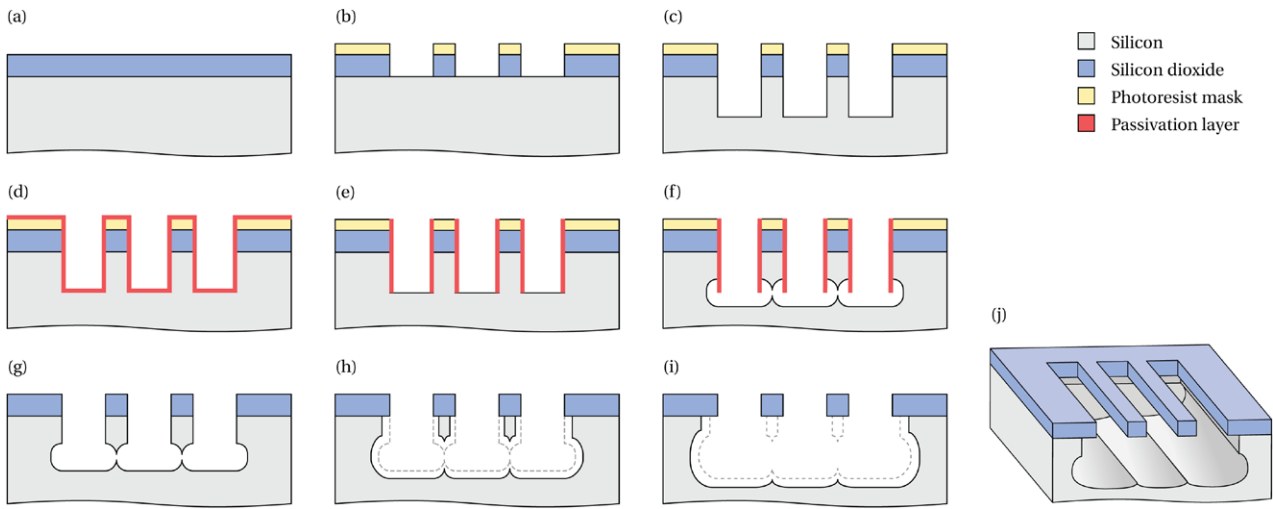


**Figure 1.** Fabrication steps for the release of reinforced structures. (a) Starting material: Si wafer with thermal SiO<sub>2</sub>. (b) Photoresist patterning and plasma etching through SiO<sub>2</sub>. (c) DRIE of Si. (d) Deposition of passivation layer. (e) Removal of the passivation layer from the trench bottom. (f) Isotropic plasma etching of Si. (g) Removal of the passivation layer and photoresist mask results in released SiO<sub>2</sub> beam structures with Si support. Optionally, the supporting Si can be removed by additional steps: (h) Isotropic plasma etching of Si. (i) Continued isotropic plasma etching of Si. (j) 3D representation of the end result: suspended SiO<sub>2</sub> structures.

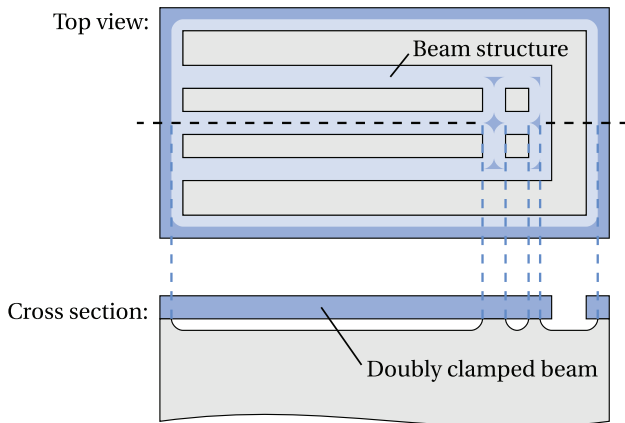


**Figure 2.** Schematic representation of a SiO<sub>2</sub> beam structure during the underetching process without Si reinforcement.

reinforcement. Figure 2 illustrates the state at a certain moment during the underetching of a SiO<sub>2</sub> beam structure without Si reinforcement. In this figure, the beam structure is almost entirely suspended. Only at the beam crossings, the SiO<sub>2</sub> is attached to the Si wafer. Due to the geometry of the beam structure, the release of the beams occurs before the beam crossings are released. The three beams, being suspended but also clamped at both ends (at their base and at the beam crossings), are actually doubly-clamped beams. These SiO<sub>2</sub> bridges, no longer supported by any Si, will expand and buckle, leading to stress concentrations and possibly beam failure.

Figure 3 illustrates the state at the same moment during the underetching of a SiO<sub>2</sub> beam structure using Si reinforcement. Again, the beam structure is suspended everywhere except at the beam crossings. However, the created bridges are bilayer structures instead of SiO<sub>2</sub> bridges. The supporting Si limits the expansion of the SiO<sub>2</sub>, which results in lower stress concentrations, reducing the chance of beam failure during fabrication.

The Si support is only required at a specific stage during the fabrication process, i.e. until the bilayer structure is

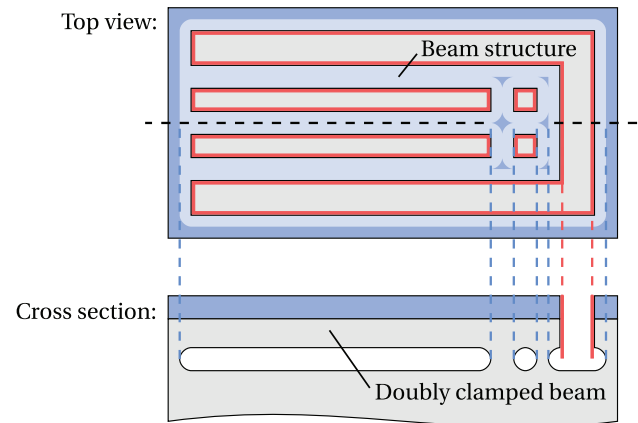


**Figure 3.** Schematic representation of a SiO<sub>2</sub> beam structure during the Si-reinforced underetching process.

released. Once the bilayer structure is fully suspended (i.e. when the beam crossings are also suspended), the supporting Si is no longer necessary. Any compressive stress remaining in the SiO<sub>2</sub> will not lead to fracturing when the supporting Si is removed since restrictions of longitudinal strain no longer exist.

In addition to the delayed release of beam crossings, another beam failure mechanism can be identified. Although isotropic etching is by definition a process with similar etch rates in all directions, the ‘isotropic’ plasma etch that was used in this study appeared to not be perfectly isotropic. For example, the etching of a rectangular window revealed a lower underetch rate in the corners compared to the underetch rate at the middle of the straight sections. This etch anisotropy caused doubly-clamped beam situations during the underetching of cantilever beams. Si reinforcement reduces the risk of cantilever beam fracturing caused by local etch rate differences. Similar to the situation depicted in figure 3, any doubly-clamped beams formed during underetching will be reinforced by the supporting Si.

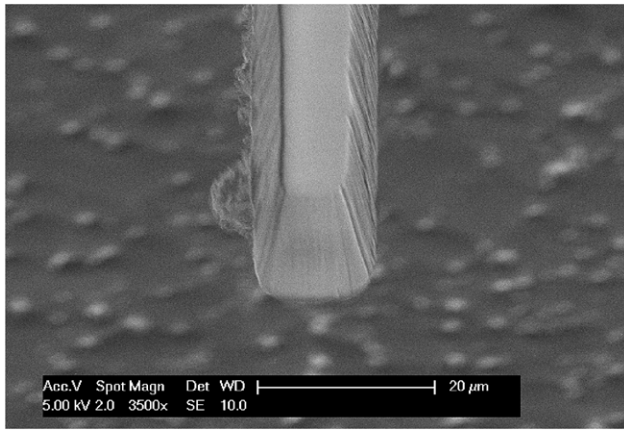


**Figure 4.** Scanning Electron Microscope (SEM) image of a suspended  $\text{SiO}_2$  beam, with the end facet of the beam in the center of the image. This image was acquired with a tilted stage.

## 2.2. Design

In order to test the effect of Si reinforcement on structures with and without beam crossings, the design included individual waveguide beams and waveguide beams connected at their free ends by a crossbar. The individual beams were designed in sets of one, two, and four parallel beams; the connected structures consisted of two and four parallel beams. All the beam structures were designed with a variety of lengths (250  $\mu\text{m}$ , 500  $\mu\text{m}$ , 750  $\mu\text{m}$ , 1000  $\mu\text{m}$ ) and widths (18  $\mu\text{m}$ , 26  $\mu\text{m}$ , 34  $\mu\text{m}$ ). These dimensions are a trade-off between having a sufficient cladding thickness (for low propagation loss of future photonic waveguide beams) and obtaining a low bending stiffness (in order to position the beams using micro-actuators). Furthermore, test cantilevers were included with a designed width of 15  $\mu\text{m}$  and a varying designed length. A single wafer contained 72 identical arrays of 60 cantilevers of which the length ranged from 10  $\mu\text{m}$  to 1000  $\mu\text{m}$  with a step size of 16.5  $\mu\text{m}$ .

## 3. Results and discussion

### 3.1. Released structures

The realized structures were measured to be approximately 5  $\mu\text{m}$  less wide than designed, resulting in 13  $\mu\text{m}$ , 21  $\mu\text{m}$ , 29  $\mu\text{m}$  wide beams and 10  $\mu\text{m}$  wide test cantilevers. The etch profile had a positive taper between  $9^\circ$  and  $10^\circ$ , resulting in a trapezoidal cross section of the  $\text{SiO}_2$  beams. Figure 4 shows an angled view of one of the fabricated  $\text{SiO}_2$  beams. The beam widths mentioned above are the mean values of the narrow top and the wider bottom of this trapezoid. The exact cause of the difference between the designed and the obtained width is under investigation. All the final structures had a measured thickness of 14  $\mu\text{m}$ , roughly 0.8  $\mu\text{m}$  less than the  $\text{SiO}_2$  thickness at the start of the fabrication. This means that approximately 0.8  $\mu\text{m}$  of  $\text{SiO}_2$  was etched from the top surface after removal of the photoresist mask.

Figures 5 and 6 show four parallel suspended beams with and without supporting Si, respectively. The  $\text{SiO}_2$  beams in both figures are 1000  $\mu\text{m}$  in length and 13  $\mu\text{m}$  in width.

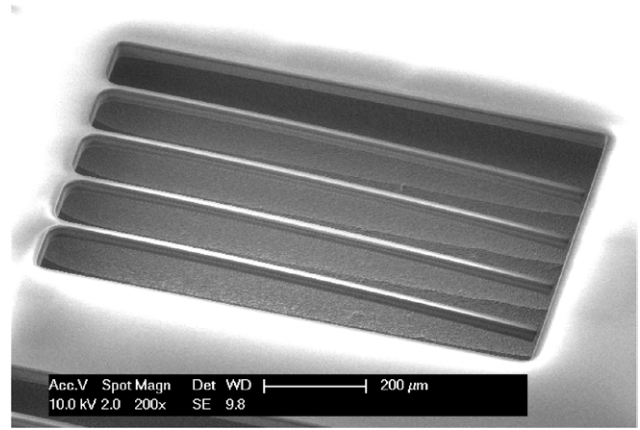


**Figure 5.** SEM image of suspended bilayer beams.

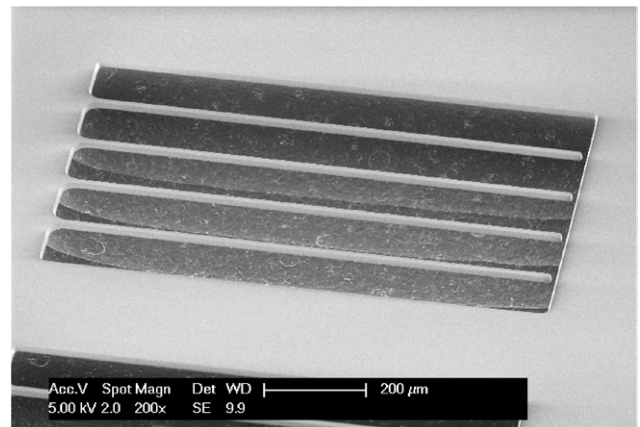


**Figure 6.** SEM image of suspended  $\text{SiO}_2$  beams.

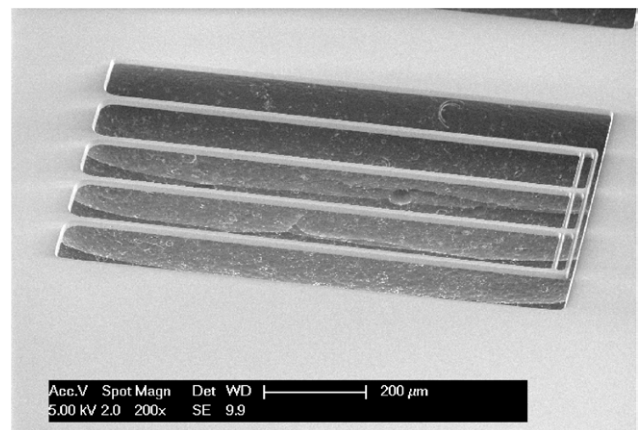


**Figure 7.** SEM image of suspended  $\text{SiO}_2$  structure consisting of four beams, connected at their free ends.

Furthermore, suspended structures consisting of parallel waveguide beams, connected by a crossbar, were fabricated. Figure 7 shows a suspended  $\text{SiO}_2$  structure consisting of 4 connected waveguide beams, each 1000  $\mu\text{m}$  long and 13  $\mu\text{m}$  wide.

The fabrication yield of single cantilevers was determined by counting the number of truncated test cantilevers. Based on a single wafer with 4320 cantilevers in total, an overall yield of 97.8% was observed. Up to a length of 750  $\mu\text{m}$ , all

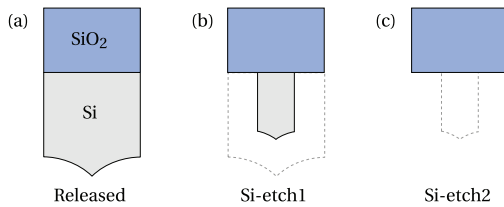


**Figure 8.** Schematic cross sections of a waveguide beam at the three measurement moments during the release process: (a) after the initial release; (b) after 60 s of etching the supporting Si; (c) after 210 s of additionally etching the supporting Si layer.

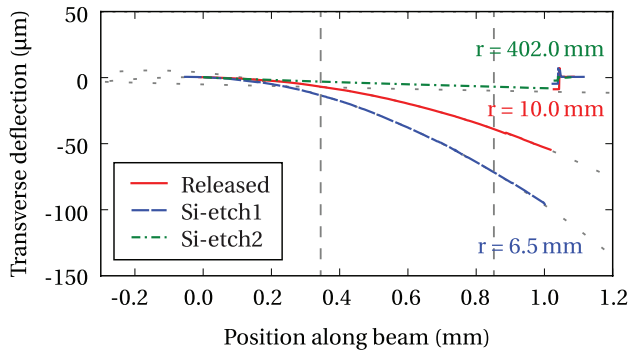


**Figure 9.** Measured deflections of a single cantilever at the three states during fabrication. The cantilever was 1000  $\mu\text{m}$  long, 21  $\mu\text{m}$  wide and 14  $\mu\text{m}$  thin. The segment of the profiles between the dashed vertical lines was curve-fitted with a circle, and the corresponding radii of curvature are included in the plot. The top surface of the chip corresponds with a transverse deflection value of 0  $\mu\text{m}$ . The profile measured after Si-etch2 has a negative slope at the base and a curvature in the direction opposite to the curvatures measured at the other states (not visible at the scale of the plot).

cantilevers were intact. Above this length, the number of truncated cantilevers increased with the cantilever length. The most affected cantilevers were the longest ones, resulting in a yield of 83% for the 1000  $\mu\text{m}$  long cantilevers.

As opposed to the test cantilevers, the beam structures only showed incidental beam failure. This can be explained by the fact that they consist of beams that are wider than the test cantilevers, making them less fragile. Because of the large variation in beam length and beam width of the structures, the number of implementations of one version was limited. As a consequence, the number of realized beam structures of a specific size was too low to estimate the corresponding yield with any degree of confidence.

### 3.2. Beam deflection

This section discusses the initial out-of-plane bending of the suspended beams, which was caused by residual stress originating from the thermal oxidation. The profiles of cantilever beams were measured at room temperature using white light interferometric profilometry. A Bruker Contour GT-K 3D optical profilometer was used. Measurements were performed at three different moments during the fabrication process. The first measurement was performed after the release of the bilayer beam, the second after partly etching the supporting Si (i.e. 60 s of etching), and the third after fully etching the

supporting Si (i.e. another 210 s of etching). These three states correspond to steps (g)–(i) in figure 1 and will be referred to as ‘Released’, ‘Si-etch1’, and ‘Si-etch2’, respectively. Figure 8 schematically illustrates the cross sections at the three measured moments during fabrication.

The transverse deflection measurements (of which one example is presented in figure 9) show that the profile of the beam is different at the three fabrication states. The maximum deflection of the free end occurred after Si-etch1, and was almost 100  $\mu\text{m}$ . The beam curvatures were retrieved by curve-fitting the measured profiles with a circle. Only the relevant part of every measurement was used for the curve fitting, indicated by the dashed vertical lines in figure 9. From the measured beam profiles two deformation effects can be distinguished.

**3.2.1. Beam curvature.** The first effect is an out-of-plane deflection with a constant radius of curvature, which was dependent on the amount of supporting Si. The curvature of the bilayer beams corresponded to a concave downward ( $\cap$ ) profile for both the released and Si-etch1 state. However, the SiO<sub>2</sub> beams revealed a small curvature in the opposite direction (concave upward,  $\cup$ ).

The curvature at the different states during the release process depends on the configuration of and the residual stress in the bilayer beam. Residual stresses originate from the high temperature oxidation and the subsequent cooling down to room temperature in combination with the different thermal expansion coefficients of SiO<sub>2</sub> and Si. As a consequence, the bilayer beam will show a curvature.

The amount of curvature is a non-linear function of the Si layer thickness. At the Released state (see figure 9), there will be a certain concave downward curvature, caused by the prevailing Si and SiO<sub>2</sub> thickness. Etching of the Si reduces its thickness. In addition, the Si is also etched from the sides, reducing its width and resulting in an irregular cross-sectional shape, defined by the progressing etch fronts. These effects reduce the area moment of inertia of the Si layer and, as a consequence, the concave downward curvature increases during etching (Si-etch1 in figure 9). At small dimensions of the Si layer, the SiO<sub>2</sub> layer becomes dominant in the mechanics of the beam, and the curvature decreases with etching of Si. When all the Si is etched, the SiO<sub>2</sub> beam shows a small concave upward curvature (Si-etch2 in figure 9), which is caused by the intrinsic gradient stress present in thermal SiO<sub>2</sub> [11, 12].

**3.2.2. Slope at the base of the beam.** The second effect is a negative slope at the base of the cantilever. At this location the Si under the cantilever is removed, leaving a Si sidewall beneath the cantilever base. The compressive and gradient stress in the SiO<sub>2</sub> lead to deformation of the SiO<sub>2</sub> near this Si sidewall. If a pure SiO<sub>2</sub> cantilever is considered, the SiO<sub>2</sub> layer is free to expand at its top, but is constrained by the stiff Si, which causes the initial negative slope. For the SiO<sub>2</sub> beams, a negative slope of approximately 0.5° was observed. The initial slope of bilayer beams was smaller with increasing thickness of supporting Si.

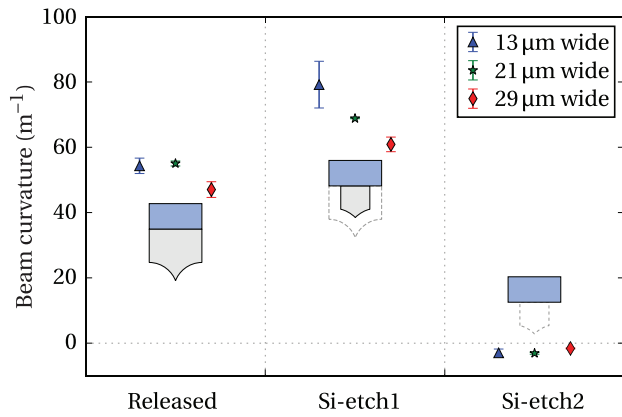


**Figure 10.** Beam curvatures measured at the different states during the release process. The error bars indicate the standard deviation from the mean value. This plot only includes the cantilevers with a narrow etch trench ( $\sim 30 \mu\text{m}$ ).

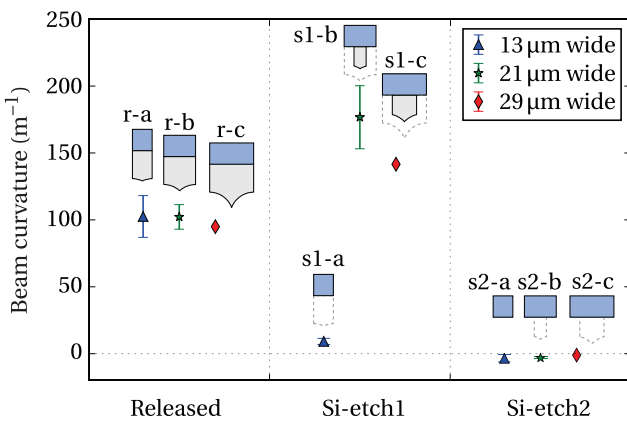


**Figure 11.** Beam curvatures measured at the different states during the release process. The error bars indicate the standard deviation from the mean value. This plot only includes the cantilevers with a wide etch trench ( $\sim 100 \mu\text{m}$ ).

**3.2.3. Mean beam curvatures.** The mean curvatures as a function of Si reinforcement of measured beam arrays (consisting of either four separate or connected beams) with a length of  $250 \mu\text{m}$ ,  $500 \mu\text{m}$ ,  $750 \mu\text{m}$ ,  $1000 \mu\text{m}$  are presented in two separate figures. Figure 10 shows the mean curvatures of beams underetched with a narrow trench ( $\sim 30 \mu\text{m}$ ), while figure 11 includes the mean curvatures resulting from a wide etch trench ( $\sim 100 \mu\text{m}$ ). In both figures, a positive curvature corresponds to a concave downward profile. It is observed that the narrower trench resulted in a lower underetch rate, causing an increased degree of Si reinforcement after the same etch duration.

The curvature of the bilayer beams does not depend on the length. It does depend on the beam width, as can be seen in both figures. This can be explained by the differences in Si support. Different beam widths result in different cross sections of the Si part, affecting the curvature.

An unexpected observation is that the curvatures of the  $13 \mu\text{m}$  wide beams after Si-etch1 (s1-a in figure 11) are much smaller than those of the wider beams (s1-b and s1-c in figure 11). Moreover, the beams with a similar width, but released using a narrow trench, do not show this decrease in curvature (see figure 10). The reason for this inconsistency

**Table 1.** Determined out-of-plane bending stiffness values (mean and standard deviation) of  $\text{SiO}_2$  cantilevers.

Length ( $\mu\text{m}$ )	Width ( $\mu\text{m}$ )	Stiffness ( $\text{N m}^{-1}$ )	
		mean	s
250	13	53.7	1.6
	21	73.1	1.7
	29	93.6	0.8
500	13	6.9	0.1
	21	9.5	0.1
	29	12.2	< 0.1
750	13	2.1	< 0.1
	21	2.9	< 0.1
	29	3.8	< 0.1
1000	13	0.8	n/a
	21	1.2	< 0.1
	29	1.6	< 0.1

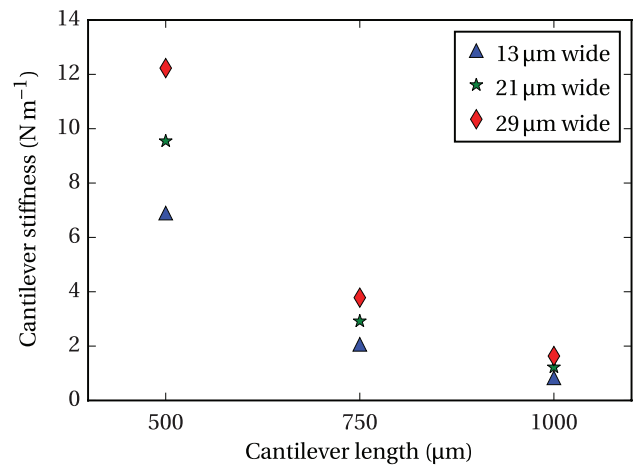


**Figure 12.** Determined out-of-plane beam bending stiffness of  $\text{SiO}_2$  cantilevers (not Si-reinforced) as a function of beam length, plotted for different cantilever widths.

is that a wider etch trench causes a higher etch rate. The  $13 \mu\text{m}$  wide beams no longer have any Si reinforcement after Si-etch1, if they are released using a wide trench. However, the wider beams (s1-b and s1-c) are still supported by Si after Si-etch1, as well as the beams of similar width that are released using a narrow trench.

**3.3. Beam bending stiffness**

This section describes the bending stiffness of the  $\text{SiO}_2$  beams. In the application of photonic alignment, integrated MEMS actuators will be implemented to position the array of waveguide beams. Because the available force of MEMS actuators is limited, the waveguide array should have a low bending stiffness. In order to obtain a rough estimate of the desired stiffness, one can imagine a microactuator capable of delivering  $1 \text{ mN}$ . The out-of-plane positioning of a waveguide array over a range of  $5 \mu\text{m}$  requires a maximum array stiffness of  $200 \text{ N m}^{-1}$ . In case the waveguide array comprises ten parallel beams, this corresponds to an out-of-plane bending stiffness of individual beams of approximately  $20 \text{ N m}^{-1}$ .

The bending stiffness can be determined using the relation

$$k = m_{\text{eff}}(2\pi f)^2, \quad (1)$$

where  $k$  is the bending stiffness,  $m_{\text{eff}}$  is the effective mass, and  $f$  is the natural resonance frequency. The out-of-plane natural resonance frequency was measured with laser Doppler vibrometry at ambient conditions. The effective mass was based on dimensions which were estimated from scanning electron microscope (SEM) images.

The determined out-of-plane bending stiffness values of SiO<sub>2</sub> cantilevers (not Si-reinforced) are presented in table 1 and depicted in figure 12. The values for a length of 250 μm are included in the table, but are not shown in the graph, since they are not compatible with the photonic alignment concept. The determined bending stiffness values corresponding to a cantilever of 250 μm in length are greater than 50 N m<sup>-1</sup>. As seen in the rough calculation above, those stiffness values are outside our range of interest. All cantilevers with a length of 500 μm or more have a derived bending stiffness smaller than 20 N m<sup>-1</sup> and therefore satisfy our stiffness requirement.

Figure 12 shows the decrease in stiffness with increasing cantilever length. The stiffness and length are related by the equation

$$k = \frac{3EI}{L^3}, \quad (2)$$

where  $k$  is the bending stiffness,  $E$  is the Young's modulus,  $I$  is the area moment of inertia, and  $L$  is the length of the cantilever. The data points in figure 12 corresponding to a specific width show a third power relationship, which is in accordance with (2).

For a specific cantilever length, the bending stiffness is expected to scale linearly with the cantilever width, because the area moment of inertia is proportional to the width. For a rectangular beam, the area moment of inertia is

$$I = \frac{1}{12}bh^3, \quad (3)$$

with  $I$ ,  $b$ , and  $h$  the area moment of inertia, the beam width and the beam height, respectively. The determined data show a deviation from this linear relation of up to 15%. This can be explained by the trapezoidal shape of the cross-sections of the beams.

As described in this paper, suspended structures of thick SiO<sub>2</sub> were realized. Their compatibility with microactuators in terms of stiffness proved to be mostly dependent on the cantilever length. Follow-up experiments will include the integration of microactuators with functional suspended waveguide beams and will involve optical characterization. We expect that the optical properties of suspended waveguide beams will be affected by the SiO<sub>2</sub> etch. Properties like the sidewall surface roughness and the etch taper will influence the performance at the waveguide end facet (e.g. scattering and propagation direction of the guided light).

#### 4. Conclusion

This paper has presented a robust microfabrication process for the release of SiO<sub>2</sub> structures. This novel process

reinforces the SiO<sub>2</sub> with Si, thereby reducing the risk of beam fracturing. Moreover, the fabrication process allows for a configurable thickness of the final Si support. The advantages of the Si reinforcement are control over the beam stiffness and a greatly enhanced design freedom for suspended SiO<sub>2</sub> structures. The fabrication yield was 97.8% for cantilever beams with a thickness of 14 μm, a width of 10 μm and a length ranging from 10 μm to 1000 μm. In addition to cantilever beams, more complex structures were successfully realized, consisting of parallel beams, connected by a crossbar at their free end.

The bilayer beams were measured to have a concave downward profile with a constant radius of curvature, which was observed to change as a function of Si support. SiO<sub>2</sub> beams without supporting Si were found to have a concave upward profile and a much smaller curvature. A 1000 μm long bilayer beam of 21 μm width was observed to have a radius of curvature of 10 mm after its release. Partly etching the supporting Si resulted in a smaller curvature, corresponding to a radius of curvature of 6.5 mm. After complete removal of the supporting silicon, the cantilever showed a concave upward profile with a radius of curvature of 402 mm.

The measured out-of-plane bending stiffness of the SiO<sub>2</sub> beams ranged from roughly 1 N m<sup>-1</sup>–100 N m<sup>-1</sup>. The long beams (i.e. 500 μm and longer) are compliant enough to be positioned by microactuators. The short beams, however, are probably too stiff to be positioned by microactuators within the required motion range.

To explore a more extensive application of Si reinforcement, future research will include experiments with more complex material configurations. A relevant follow-up experiment will be the realization of suspended functional waveguides (i.e. TriPleX waveguides with Si<sub>3</sub>N<sub>4</sub> core). Subsequently, a SiO<sub>2</sub>-based MEMS application will be realized by adding microactuators to the SiO<sub>2</sub> photonic waveguides.

#### Acknowledgments

The research leading to the presented results has received funding from the STW Generic Technologies for Integrated Photonics (GTIP) programme, grant no. 11355 (Flex-O-Guides). We are grateful to our colleagues at the Else Kooi Laboratory for the support in microfabrication. Furthermore, we thank J Kokorian for the assistance in the data analysis.

#### References

- [1] Henry C H, Kazarinov R F, Lee H J, Orlowsky K J and Katz L E 1987 Low loss Si<sub>3</sub>N<sub>4</sub>-SiO<sub>2</sub> optical waveguides on Si *Appl. Opt.* **26** 2621–4
- [2] Morichetti F, Melloni A, Martinelli M, Heideman R G, Leinse A, Geuzebroek D H and Borreman A 2007 Box-shaped dielectric waveguides: a new concept in integrated optics? *J. Lightwave Technol.* **25** 2579–89
- [3] Peters T-J, Tichem M and Stauffer U 2014 Suspended photonic waveguide arrays for submicrometer alignment *Proc. SPIE: Int. Soc. Opt. Eng.* **9133** 913317

- [4] Liu H B and Chollet F 2009 Moving polymer waveguides and latching actuator for  $2 \times 2$  MEMS optical switch *J. Microelectromech. Syst.* **18** 715–24
- [5] Kelly D P, Pruessner M W, Amarnath K, Datta M, Kanakaraju S, Calhoun L C and Ghodssi R 2004 Monolithic suspended optical waveguides for InP MEMS *IEEE Photonics Technol. Lett.* **16** 1298–1300
- [6] Stuart H R, Baumann F H and Wong-Foy A 2004 Monolithic integration of optical waveguides and MEMS-based switching in silicon-on-insulator *Proc. SPIE: Int. Soc. Opt. Eng.* **5347** 137–44
- [7] Carpenter L G, Holmes C, Rogers H L, Smith P G R and Gates J C 2010 Integrated optic glass microcantilevers with bragg grating interrogation *Opt. Express* **18** 23296–301
- [8] Ollier E 2002 Optical MEMS devices based on moving waveguides *IEEE J. Sel. Top. Quantum Electron.* **8** 155–62
- [9] Chen L, Doerr C R, Chen Y K and Liow T Y 2010 Low-loss and broadband cantilever couplers between standard cleaved fibers and high-index-contrast  $\text{Si}_3\text{N}_4$  or Si waveguides *IEEE Photonics Technol. Lett.* **22** 1744–6
- [10] Wang W-C, Fauver M, Ho J N, Seibel E J and Reinhall P G 2002 Micromachined optical waveguide cantilever as a resonant optical scanner *Sensors Actuators A* **102** 165–75
- [11] Fitch J T, Bjorkman C H, Lucovsky G, Pollak F H and Yin X 1989 Intrinsic stress and stress gradients at the  $\text{SiO}_2/\text{Si}$  interface in structures prepared by thermal oxidation of Si and subjected to rapid thermal annealing *J. Vac. Sci. Technol. B* **7** 775–81
- [12] Mrstik B J, Revesz A G, Ancona M and Hughes H L 1987 Structural and strain-related effects during growth of  $\text{SiO}_2$  films on silicon *J. Electrochem. Soc.* **134** 2020–7